Supplementary Information

Bioluminescence-activated deep-tissue photodynamic therapy of cancer

*Yi Rang Kim[1,2,3], Seonghoon Kim[1], Jin Woo Choi[4,5], Sung Yong Choi[2], Sang-Hee Lee[2], Homin Kim[2], Sei Kwang Hahn[6], Gou Young Koh[1,2], and Seok Hyun Yun[1,5,7]**

[1] Graduate School of Nanoscience and Technology (WCU), Korea Advanced Institute of Science and Technology, 291 Daehak-Ro, Yusong-Gu, Daejon 305-701, Korea

[2] Graduate School of Medical Science and Engineering, Korea Advanced Institute of Science and Technology, 291 Daehak-Ro, Yusong-Gu, Daejon 305-701, Korea

[3] Department of Oncology, Asan Medical Center, Univ. Ulsan College of Medicine, Seoul , Korea

[4] Department of Pharmacology, Wonkwang Institute of Dental Research, School of Dentistry, Wonkwang University, Iksan, Chonbuk, 570-749, Korea

[5] Wellman Center for Photomedicine, Massachusetts General Hospital, 65 Landsdowne St. UP-525, Cambridge, MA 02139, USA

[6] Department of Materials Science and Engineering, Pohang University of Science and Technology (POSTECH), 77 Cheongam-ro, Nam-gu, Pohang, Gyeongbuk 790-784, Korea.

[7] Department of Dermatology, Harvard Medical School, Massachusetts General Hospital, 40 Blossom St. Boston, MA 02114, USA

*Corresponding Author:
S. H. Andy Yun, Ph.D.
Associate Professor
Tel: 1-617-768-8704
Email: syun@mgh.harvard.edu

Supplementary Information

Photomedicine Various light-based technologies have been developed for diagnosis and treatment. Fluorescence imaging has shown great promise in the early detection of diseases because of its high sensitivity and molecular specificity *in vivo* (Ntziachristos et al., 2005; Weissleder and Mahmood, 2001). Optically controlled treatment methods, such as photodynamic therapy (PDT) (Castano et al., 2006; Hamblin and Hasan, 2004; von Maltzahn et al., 2009), low-level light therapy (Huang et al., 2009), controlled drug release (Yavuz et al., 2009), and photochemical tissue bonding (Kamegaya et al., 2005), utilize the photothermal and photochemical effects of light on cells and molecules. These techniques are rapidly emerging, while PDT in particular is widely used in ophthalmology and oncology (Agostinis et al., 2011). In addition, new ground-breaking tools, such as optogenetics (Boyden et al., 2005) and light-controlled synthetic biology (Ye et al., 2011), continue to emerge. Fiber-optic catheters can bring a light source closer to the tissue in the body; however, delivering the light further into the deeper target remains a challenge. To date, the clinical applications of light-based techniques have been limited to the superficial tissues in the skin or eye or to the epithelial surfaces of internal organs.

Light penetration in tissue **Figure 1** illustrates the problem of light penetration. When light is applied to the skin topically, its penetration is limited to the epidermis and upper dermis layers (Salomatina et al., 2006). At a typical optical dose (180 J/cm^2), bleaching of the dye was observed only in the superficial layer (<1.5 mm), indicating that sufficient optical intensity was achieved only at the top surface of the skin. Increasing the light intensity is not possible, as it can cause thermal damage in the superficial tissue. Increasing the illumination time is not practical either. This problem of penetration depth is a serious limitation for many optical techniques. For example, photochemical tissue bonding is a promising method for scar-less wound closure (Yang et al., 2012), but its application to full-thickness (5-20 mm) skin excisions is currently not possible due to shallow illumination depths.

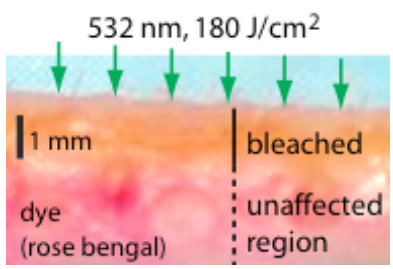

Fig. 1. Porcine skin with rose Bengal (pink) after external illumination of laser at 532 nm with 0.3 W/cm^2 for 10 min. Only the dye within the top 1.5 mm-deep region has bleached (orange region), indicating that light only reached the superficial layer.

Optical attenuation in tissue Optical penetration in tissue is fundamentally limited by absorption. Scattering contributes to illumination loss in two ways: by increasing the absorption through the increase of the propagation length in tissue and also by causing the beam to diverge. In general, light intensity decreases exponentially with depth. In the case of uniform illumination over a wide area (>10 cm^2), the attenuation can be expressed as:

$$I(z)=I_0*\exp(-\mu_{eff}*z) \qquad (1)$$

where I_0 is the input intensity. Here, the effective attenuation coefficient μ_{eff} is given by:

$$\mu_{eff}=[3*\mu_a*(\mu'_s+\mu_a)]^{1/2}, \qquad (2)$$

where μ'_s is the reduced scattering coefficient, and μ_a is the absorption coefficient of the tissue. At a wavelength (λ) of 480 nm, μ_{eff} = ~-20 cm^{-1}, and the total attenuation is $4x10^{-9}$ cm^{-1} or 84 dB/cm. That is, *to deliver one photon to z=1 cm, it is necessary to illuminate the surface with as many as 200 million photons.* The attenuation generally decreases at longer wavelengths (e.g., 30-60 dB/cm at λ=650 nm, see **Table 1**) (Cheong et al., 1990). For point sources, such as fiber-optic illumination, the optical intensity tends to decrease more rapidly with depth due to beam divergence. The experiments and the Monte Carlo simulation show that the attenuation is 18-23 dB at z=1 mm and 28-33 dB at 2 mm for λ=480-650 nm in various tissues (Yizhar et al., 2011).

λ (nm)	μ_a (cm^{-1})	μ_s' (cm^{-1})
480	5-10	15-40
650	1-3	10-35

Table 1. Optical scattering and absorption in a typical soft tissue.

<u>*Bioluminescence resonance energy transfer (BRET)*</u> Bioluminescence is a naturally occurring form of chemiluminescence in many organisms, such as the jellyfish, sea pansy, and firefly. A small-molecule substrate luciferin is oxidized in the presence of the enzyme luciferase to produce oxyluciferin and a photon (Wilson and Hastings, 1998). Bioluminescence imaging has been widely used for visualizing gene expression (Contag and Bachmann, 2002) and disease progression (Ntziachristos et al., 2005). In many organisms, light is emitted via bioluminescence resonance energy transfer (BRET). The green light emission observed in the jellyfish *Aequorea victoria* is a result of the non-radiative energy transfer from the aequorin to green fluorescent protein (GFP) (Shimomura, 2009). *Renilla reniformis*, a coral, emits bright green light by energy transfer from the interaction of luciferase (RLuc) and coelenterazine (Shimomura and Johnson, 1978) with a dimer GFP. Efficient energy transfer from RLuc to quantum dots (So et al., 2006) and from RLuc to EYFP (Hoshino et al., 2007) were demonstrated. BRET has been exploited for Ca^{2+} sensing (Martin et al., 2007), protein folding (Angers et al., 2000), and protein-protein interactions (Pfleger and Eidne, 2006).

Reference

Agostinis, P., Berg, K., Cengel, K.A., Foster, T.H., Girotti, A.W., Gollnick, S.O., Hahn, S.M., Hamblin, M.R., Juzeniene, A., Kessel, D., *et al.* (2011). Photodynamic Therapy of Cancer: An Update. Ca-a Cancer Journal for Clinicians *61*, 250-281.

Angers, S., Salahpour, A., Joly, E., Hilairet, S., Chelsky, D., Dennis, M., and Bouvier, M. (2000). Detection of beta(2)-adrenergic receptor dimerization in living cells using bioluminescence resonance energy transfer (BRET). Proceedings of the National Academy of Sciences of the United States of America *97*, 3684-3689.

Boyden, E.S., Zhang, F., Bamberg, E., Nagel, G., and Deisseroth, K. (2005). Millisecond-timescale, genetically targeted optical control of neural activity. Nature Neuroscience *8*, 1263-1268.

Castano, A.P., Mroz, P., and Hamblin, M.R. (2006). Photodynamic therapy and anti-tumour immunity. Nat Rev Cancer *6*, 535-545.

Cheong, W.F., Prahl, S.A., and Welch, A.J. (1990). A review of the optical-properties of biological tissues. Ieee Journal of Quantum Electronics *26*, 2166-2185.

Contag, C.H., and Bachmann, M.H. (2002). Advances in vivo bioluminescence imaging of gene expression. Annual Review of Biomedical Engineering *4*, 235-260.

Hamblin, M.R., and Hasan, T. (2004). Photodynamic therapy: a new antimicrobial approach to infectious disease? Photochemical & Photobiological Sciences *3*, 436-450.

Hoshino, H., Nakajima, Y., and Ohmiya, Y. (2007). Luciferase-YFP fusion tag with enhanced emission for single-cell luminescence imaging. Nature Methods *4*, 637-639.

Huang, Y.Y., Chen, A.C.H., Carroll, J.D., and Hamblin, M.R. (2009). Biphasic dose reponse in low level light therapy. Dose-Response *7*, 358-383.

Kamegaya, Y., Farinelli, W.A., Echague, A.V.V., Akita, H., Gallagher, J., Flotte, T.J., Anderson, R.R., Redmond, R.W., and Kochevar, I.E. (2005). Evaluation of photochemical tissue bonding for closure of skin incisions and excisions. Lasers in Surgery and Medicine *37*, 264-270.

Martin, J.R., Rogers, K.L., Chagneau, C., and Brulet, P. (2007). In vivo Bioluminescence Imaging of Ca(2+) Signalling in the Brain of Drosophila. Plos One *2*.

Ntziachristos, V., Ripoll, J., Wang, L.H.V., and Weissleder, R. (2005). Looking and listening to light: the evolution of whole-body photonic imaging. Nature Biotechnology *23*, 313-320.

Pfleger, K.D.G., and Eidne, K.A. (2006). Illuminating insights into protein-protein interactions using bioluminescence resonance energy transfer (BRET). Nat Methods *3*, 165-+.

Salomatina, E., Jiang, B., Novak, J., and Yaroslavsky, A.N. (2006). Optical properties of normal and cancerous human skin in the visible and near-infrared spectral range. J Biomed Opt *11*.

Shimomura, O. (2009). Discovery of Green Fluorescent Protein (GFP) (Nobel Lecture). Angew Chem-Int Edit *48*, 5590-5602.

Shimomura, O., and Johnson, F.H. (1978). Peroxidized coelenterazine, active group in photoprotein aequorin. Proceedings of the National Academy of Sciences of the United States of America *75*, 2611-2615.

So, M.K., Xu, C.J., Loening, A.M., Gambhir, S.S., and Rao, J.H. (2006). Self-illuminating quantum dot conjugates for in vivo imaging. Nature Biotechnology *24*, 339-343.

von Maltzahn, G., Park, J.H., Agrawal, A., Bandaru, N.K., Das, S.K., Sailor, M.J., and Bhatia, S.N. (2009). Computationally guided photothermal tumor therapy using long-circulating gold nanorod antennas. Cancer Research *69*, 3892-3900.

Weissleder, R., and Mahmood, U. (2001). Molecular imaging. Radiology *219*, 316-333.

Wilson, T., and Hastings, J.W. (1998). Bioluminescence. Annu Rev Cell Dev Biol *14*, 197-230.

Yang, P.G., Yao, M., DeMartelaere, S.L., Redmond, R.W., and Kochevar, I.E. (2012). Light-activated sutureless closure of wounds in thin skin. Lasers Surg Med *44*, 163-167.

Yavuz, M.S., Cheng, Y.Y., Chen, J.Y., Cobley, C.M., Zhang, Q., Rycenga, M., Xie, J.W., Kim, C., Song, K.H., Schwartz, A.G.*, et al.* (2009). Gold nanocages covered by smart polymers for controlled release with near-infrared light. Nat Mater *8*, 935-939.

Ye, H., Baba, M.D.E., Peng, R.W., and Fussenegger, M. (2011). A Synthetic Optogenetic Transcription Device Enhances Blood-Glucose Homeostasis in Mice. Science *332*, 1565.

Yizhar, O., Fenno, L.E., Davidson, T.J., Mogri, M., and Deisseroth, K. (2011). Optogenetics in neural systems. Neuron *71*, 9-34.

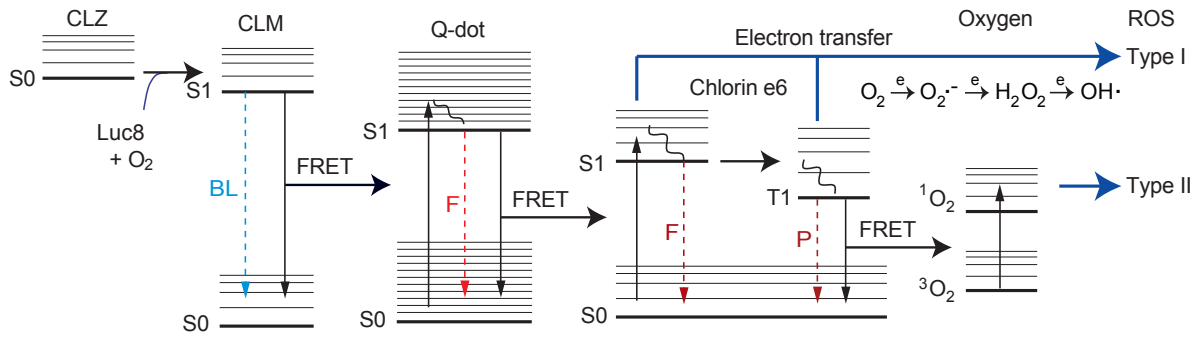

Supplementary Fig. 1: Energy diagram of the sequential Förster resonance energy transfer (FRET) from an activated coelenterazine (CTZ) to quantum dot (Q-dot or QD) to Chlorin e6, and to oxygen molecule. The end products are reactive oxygen species (ROS), through two types of processes, both of which generate cytotoxicity.

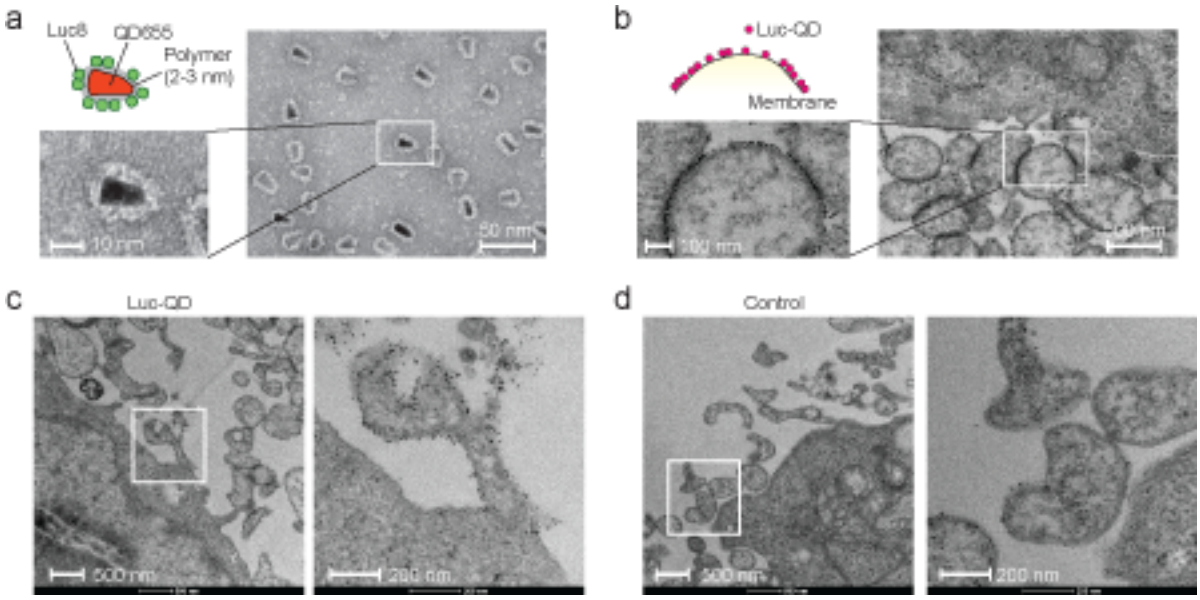

Supplementary Fig. 2: TEM images. (a) Luc-QD conjugates. The hydrodynamic diameter of the conjugate was measured to be about 20 nm. (b) Luc-QD conjugates attached to the external surface of the lipid bilayers of exosomes. (c) Cells incubated with Luc-QD for 20 min. (d) Control cells without Luc-QD.

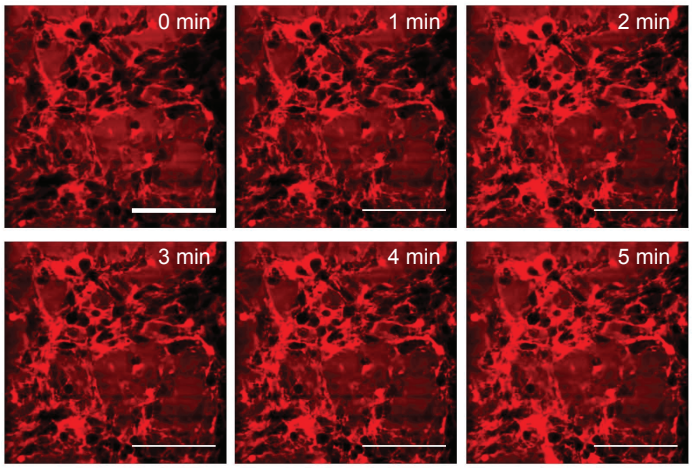

Supplementary Fig. 3: Time-lapse confocal fluorescence images of Luc-QD, showing the time-dependent accumulation of the BL source at the external surface of the cellular membrane. Scale bars, 50 μm.

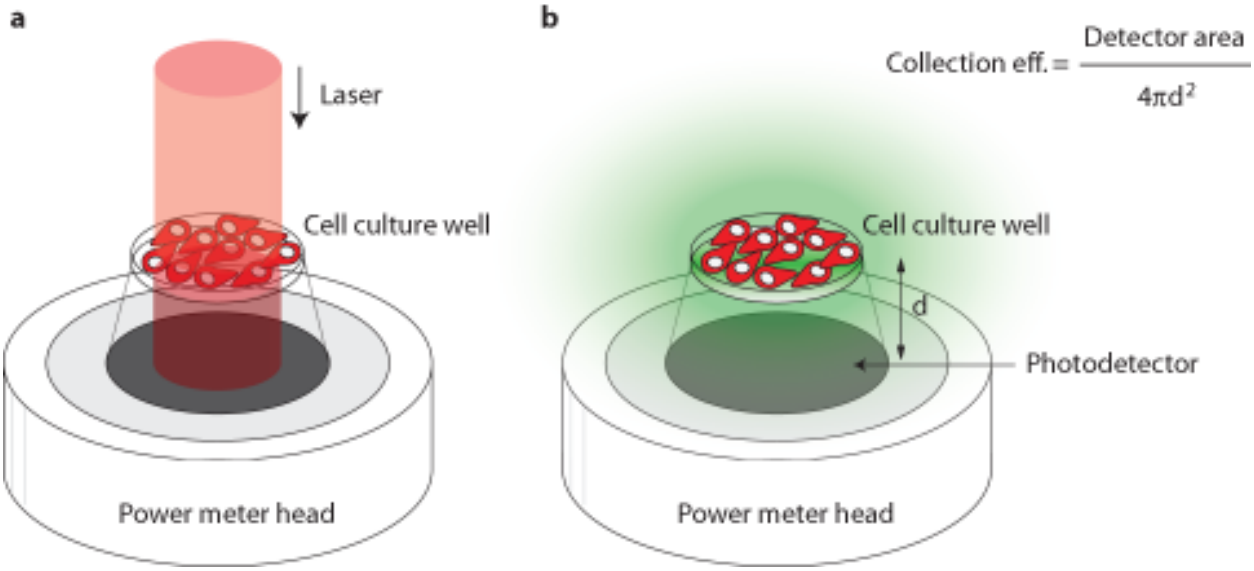

Supplementary Fig. 4: A schematic of the setup to measure the total amount of (a) laser absorption and (b) bioluminescence radiation. For the laser measurement, the incident power was 2.2 mW, and the difference in transmission through the cell culture before and after incubation with Ce6 was about 13 μW. In bioluminescence measurement, the collection efficiency is determined by the active area of the power meter head and the distance of the photodetector from the cell culture.

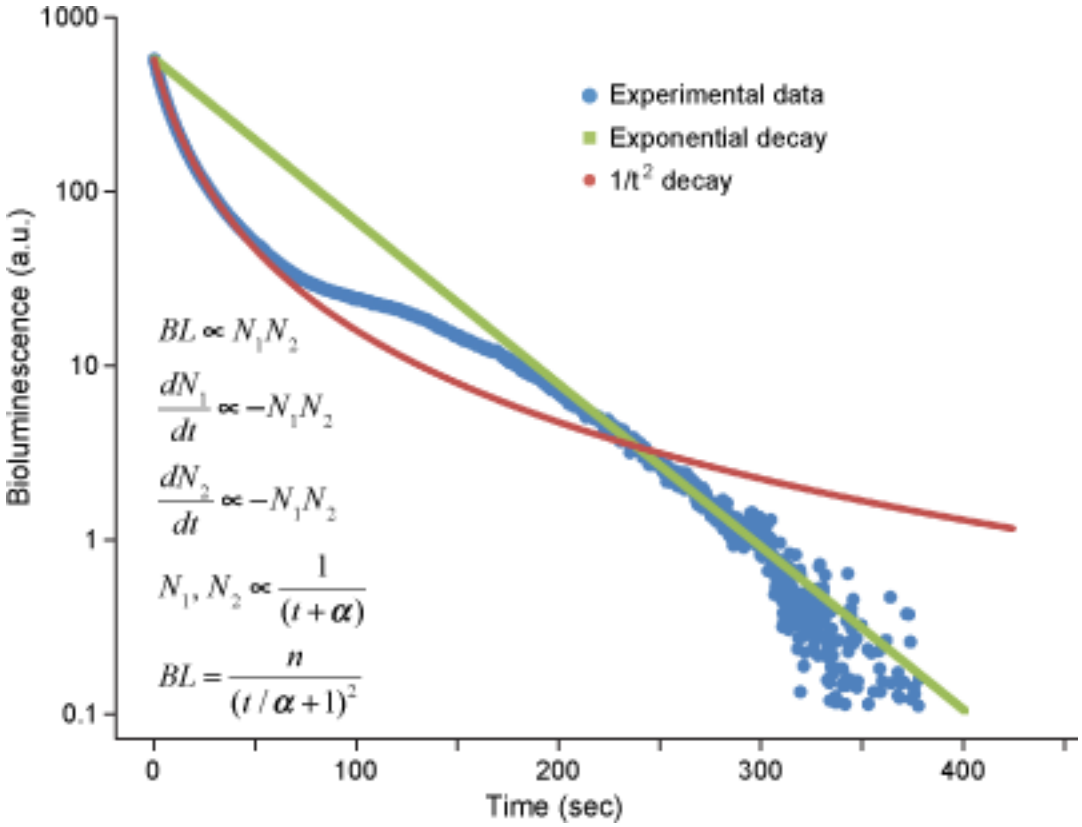

Supplementary Fig. 5: Measured bioluminescence from Luc-QD in the cell culture media. Blue circles: the measured data, Green squares: an exponential fit. Red circles: a fit with a theoretical curve derived from the rate equations. In this model, the BL intensity is proportional to the product of the number of Luc-QD (N_1) and CTZ (N_2), which is described by the first equation in the inset. Both Luc-QD and CTZ were assumed to be degraded as they reaction to produce bioluminescence, as indicated by the second and third equations. Solutions of the equations predict a 1/t-type decay of both Luc-QD and CTZ. Therefore, the BL intensity is given by the last equation in the inset. If the degradation of Luc-QD is neglected and only CTZ is depleted, the BL intensity should follow an exponential decay. The measured data are fit best with the $1/t^2$-type decay initially in the first 1-2 minutes after the injection of CTZ, suggesting a rapid consumption of Luc-QD. Later after 3 min, however, the decay seems to follow an exponential decay, indicating the remaining Luc-QD stay functional for up to several minutes.

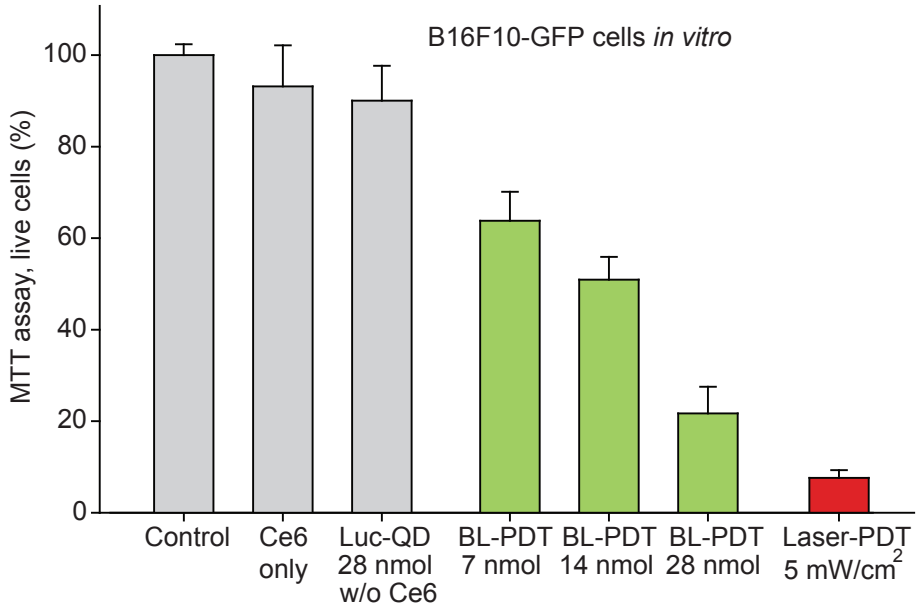

Supplementary Fig. 6: MTT assay of B16F10 cells treated with BL-PDT and laser-PDT.

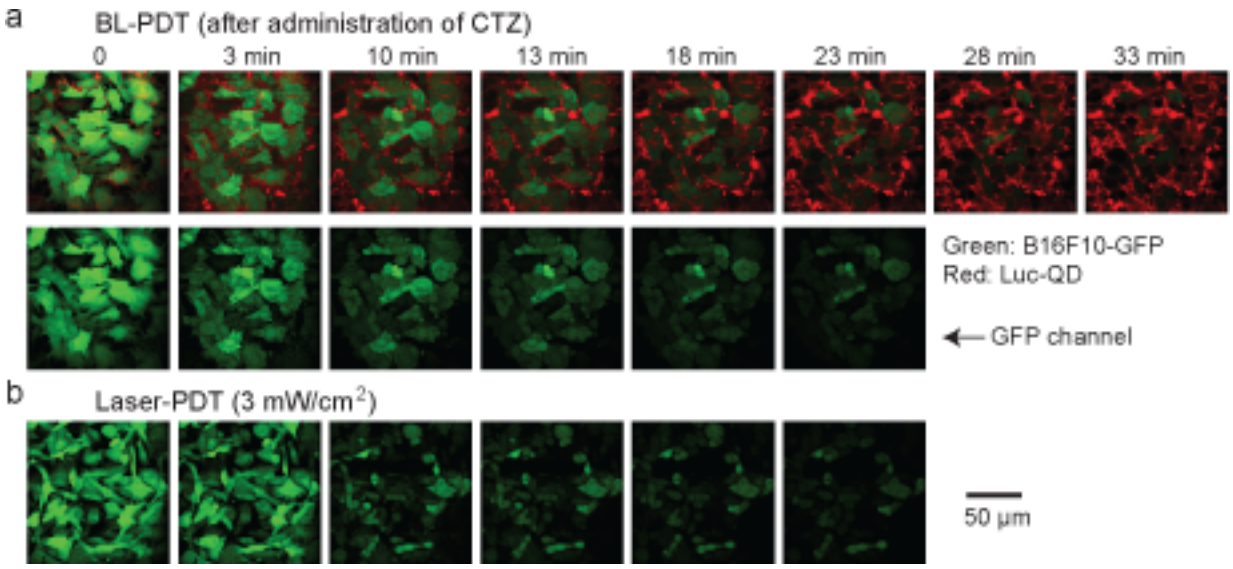

Supplementary Fig. 7: BL-PDT on B16F10-GFP melanoma cells. (a) Time-lapse confocal fluorescence images during BL-PDT. The decreases of GFP signals, accompanied by changes of cellular morphology, in both cases indicate cellular damages. The GFP signals in control cells showed no changes (not shown here). The red fluorescence increases over time during BL-PDT as the Luc-QD conjugates in the medium accumulate around the cells at the bottom of the culture well plate. (b) GFP signals during laser-PDT. Control cells without laser illumination showed no changes in GFP fluorescence intensity.

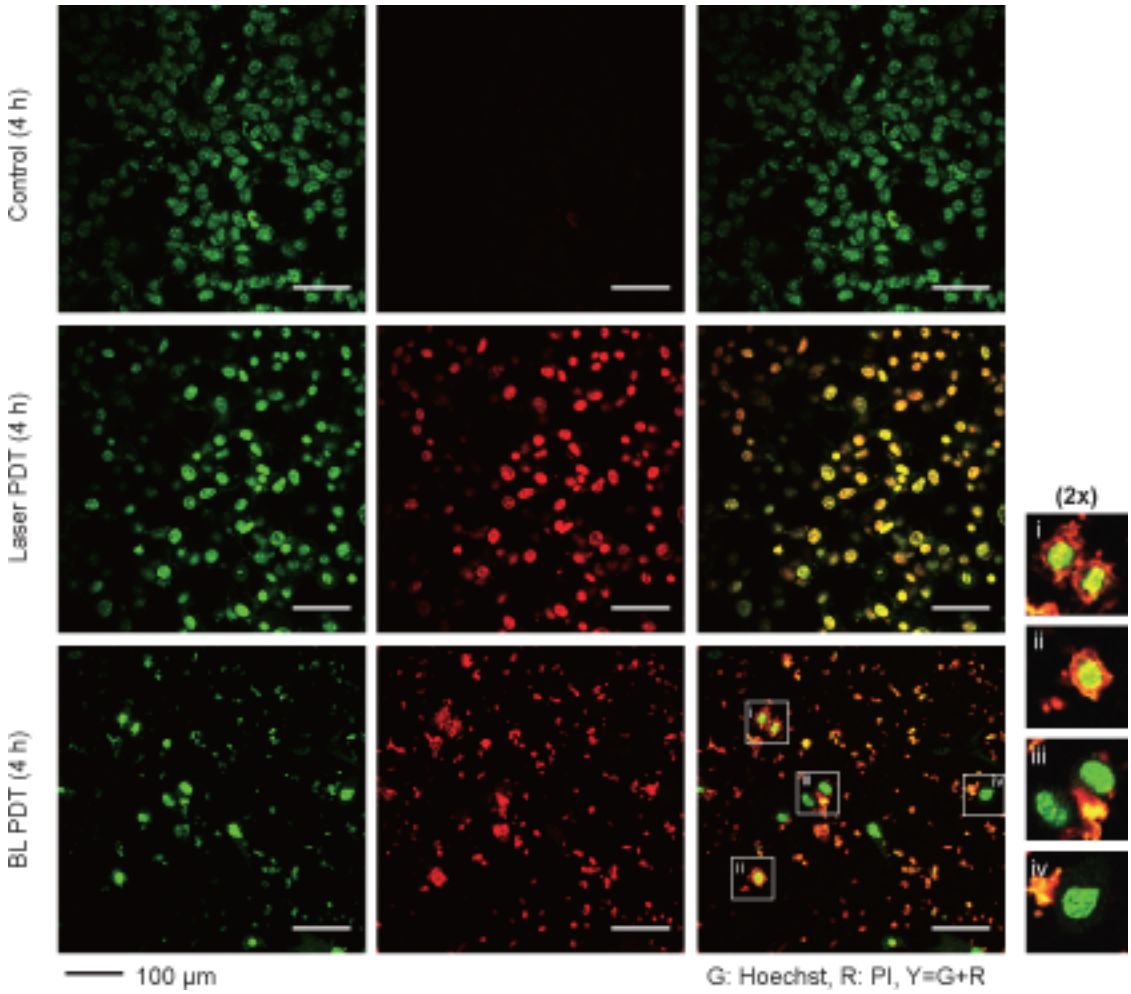

Supplementary Fig. 8: Confocal images of LLC cells after treatments. PI-positive nuclei are surrounded by large Luc-QD (i, ii), and PI-negative nuclei are with no or less Luc-QD (iii and iv).

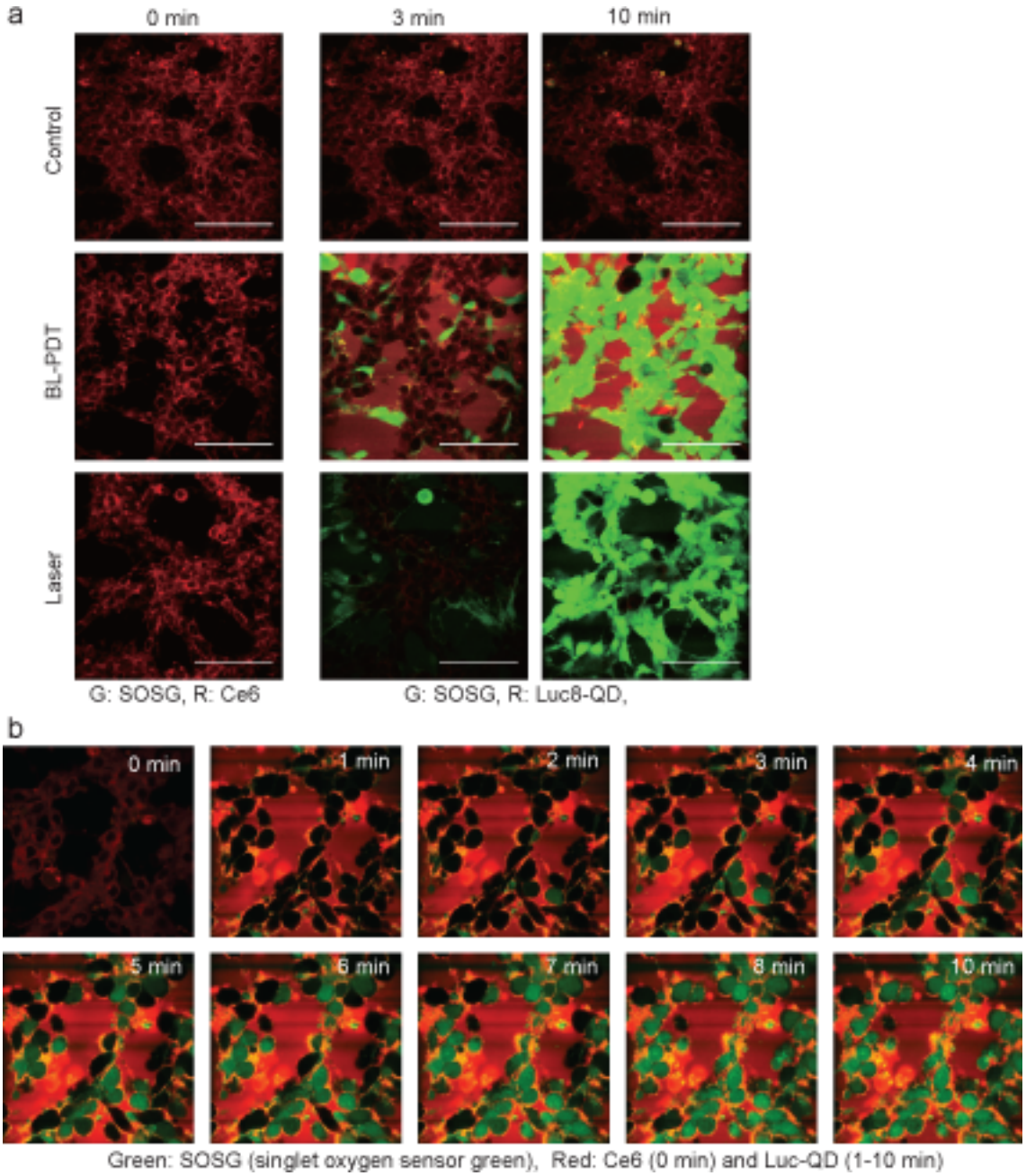

Supplementary Fig. 9: Confocal fluorescence images of Single-Oxygen-Sensor-Green (SOSG) post CTZ injection into CT26 cells *in vitro*. (a) At 0 min, SOSG are located in the culture medium outside the cells in a non-fluorescent form. At 3 min, SOSG have entered some of the cells through their damaged membranes and turned to fluorescent forms by reaction with singlet oxygen. At 10 min, most cells show green fluorescence in their cytoplasm. Scale bars, 100 µm. (b) Time-lapse confocal images of SOSG in another experiment, taken with a time interval of 1 min.

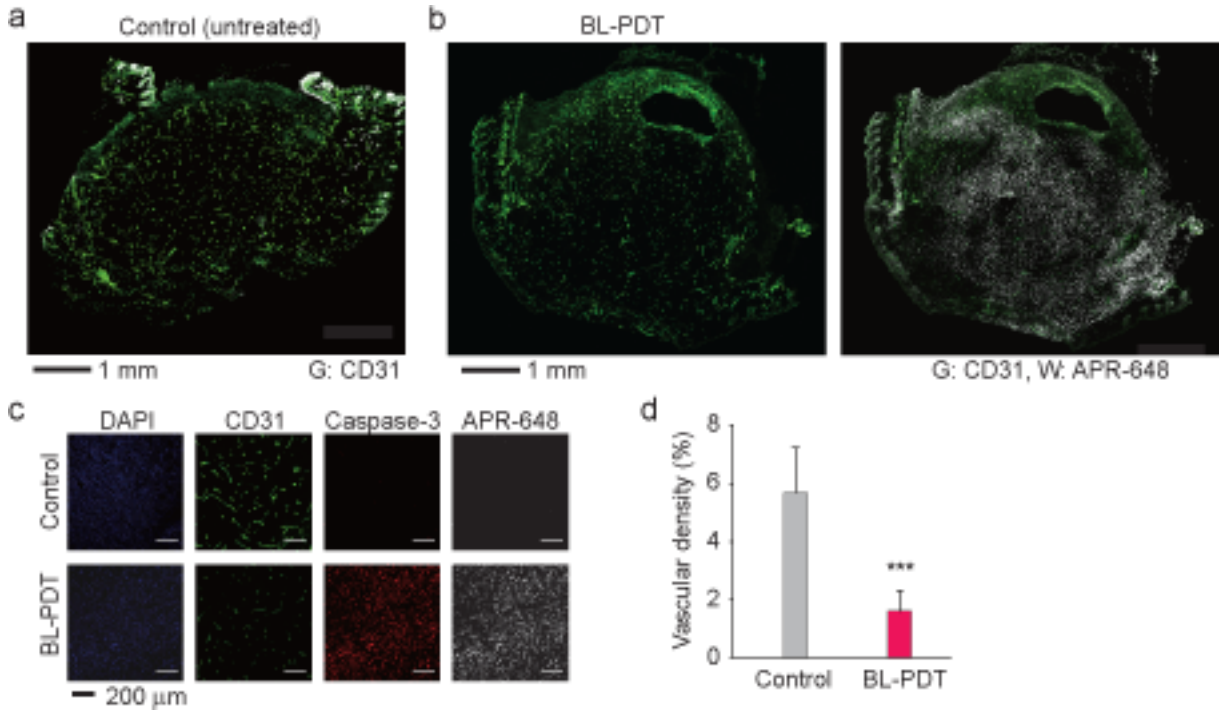

Supplementary Fig. 10: (a) Immunohistochemistry (IHC) image of an untreated tumor stained for CD31. (b) IHC images of a BL-PDT treated tumor, stained for CD31 (green) and apoptosis marker, APR-648 (white). (c) IHC for DAPI, CD31, Caspase-3 and APR-648. (d) The vascular density estimated by the CD31 signals integrated over the APR-648 positive region, indicating a significant vascular disruption by BL-PDT. ***, $p<0.001$.

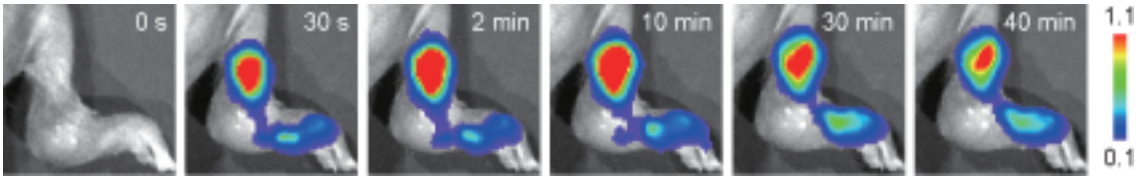

Supplementary Fig. 11: Bioluminescence images showing the draining of Luc-QD and CTZ to the popliteal LN.

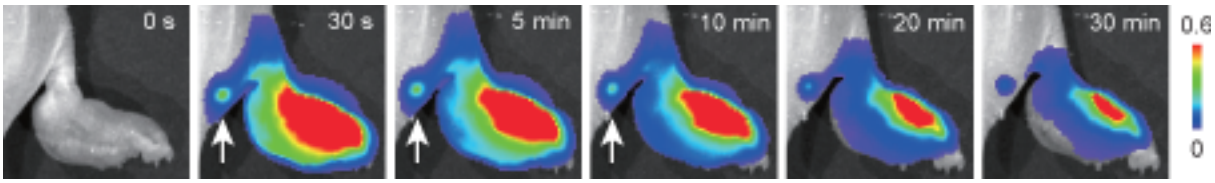

Supplementary Fig. 12: Bioluminescence images showing the draining of Luc-QD and CTZ to the lumbar LN (arrows).

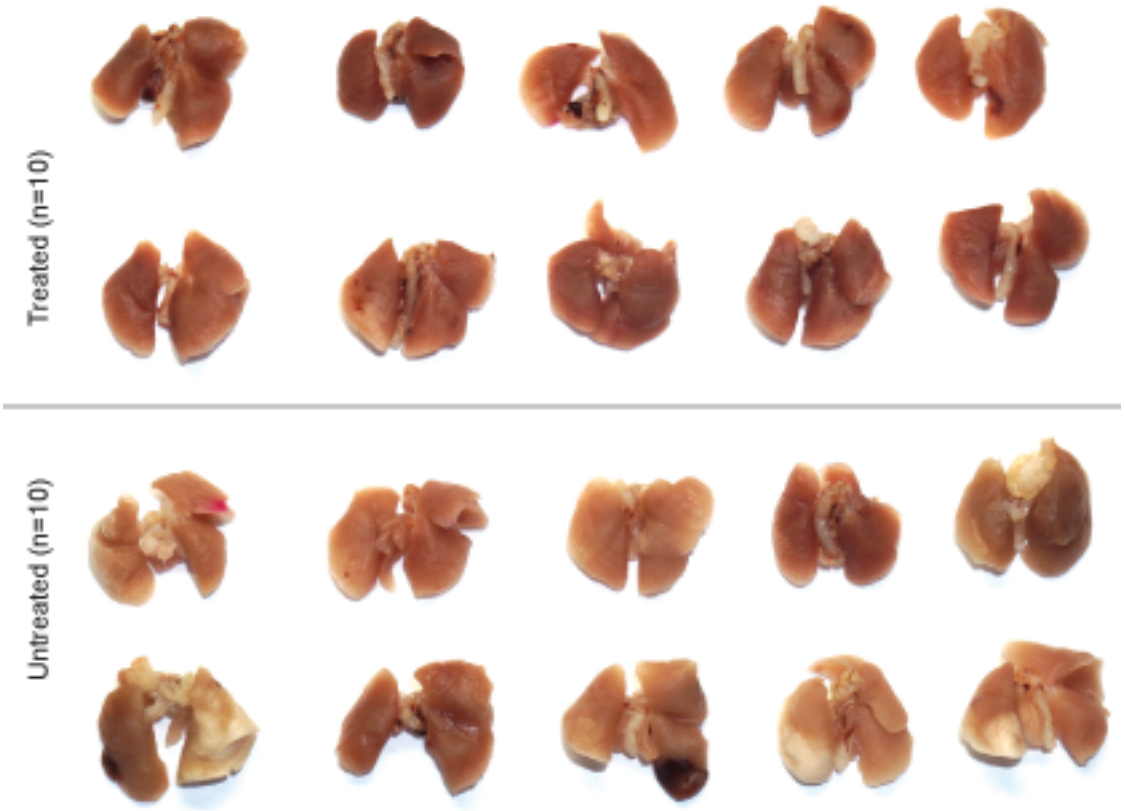

Supplementary Fig. 13: Lung samples excised from the animals at day 25 after implantation of LLC tumors in the footpad. Top, from animals treated with BL-PDT at day 11; Bottom, untreated animal group.

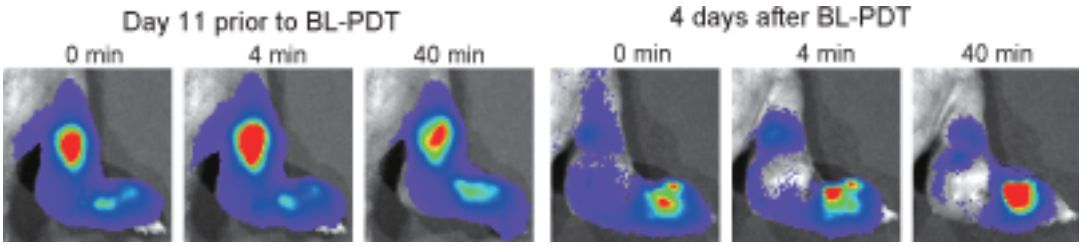

Supplementary Fig. 14: Reduced lymphatic drainage to the sentinel lymph node, observed four days after BL-PDT in a CT-26 bearing mouse.